Object and spatial mnemonic interference differentially engage lateral and medial entorhinal cortex in humans

Zachariah M. Reagh and Michael A. Yassa[1]

Department of Neurobiology and Behavior, Institute for Memory Impairments and Neurological Disorders, Center for the Neurobiology of Learning and Memory, University of California, Irvine, CA 92697-3800

Edited by Larry R. Squire, Veterans Affairs San Diego Healthcare System, San Diego, CA, and approved August 27, 2014 (received for review June 16, 2014)

Recent models of episodic memory propose a division of labor among medial temporal lobe cortices comprising the parahippocampal gyrus. Specifically, perirhinal and lateral entorhinal cortices are thought to comprise an object/item information pathway, whereas parahippocampal and medial entorhinal cortices are thought to comprise a spatial/contextual information pathway. Although several studies in human subjects have demonstrated a perirhinal/parahippocampal division, such a division among subregions of the human entorhinal cortex has been elusive. Other recent work has implicated pattern separation computations in the dentate gyrus and CA3 subregions of the hippocampus as a mechanism supporting the resolution of mnemonic interference. However, the nature of contributions of medial temporal lobe cortices to downstream hippocampal computations is largely unknown. We used high-resolution fMRI during a task selectively taxing mnemonic discrimination of object identity or spatial location, designed to differentially engage the two information pathways in the medial temporal lobes. Consistent with animal models, we demonstrate novel evidence for a domain-selective dissociation between lateral and medial entorhinal cortex in humans, and between perirhinal and parahippocampal cortex as a function of information content. Conversely, hippocampal dentate gyrus/CA3 demonstrated signals consistent with resolution of mnemonic interference across domains. These results provide insight into the information processing capacities and hierarchical interference resolution throughout the human medial temporal lobe.

The encoding of episodic memories is known to rely on a network of brain regions within the medial temporal lobes (MTL) (1). Past models of episodic memory have largely focused on the functional role of the hippocampus and its subregions. A wealth of recent evidence has implicated pattern separation, a computation by which overlapping inputs are orthogonalized into nonoverlapping outputs, as a key process in resolving interference among similar memories (2). This computation is widely thought to occur as a function of sparse firing patterns of granule cells of the hippocampal dentate gyrus (DG), which form powerful mossy fiber synapses with large numbers of pyramidal cells in subregion CA3 (3–6). A critical role for the DG in orthogonalizing interfering inputs has been demonstrated in animal studies by using lesions (7–9), NMDA receptor knockouts (10), electrophysiological recordings (11, 12), and human functional MRI (13–15).

Numerous studies have provided evidence for selective information processing in cortical areas that project to the hippocampus. Much of this research has focused on perirhinal cortex (PRC) and parahippocampal cortex (PHC, postrhinal in the rat). PRC has been shown to be critical for memory of item or object information, whereas PHC has been shown to play a role in memory of contextual or spatial information both in rats (16–18) and in humans (19–21). These dissociations are consistent with differential cortical afferentation by ventral and dorsal visual streams to PRCs and PHCs in the macaque (22). Both PRC and PHC provide input into entorhinal cortex (EC), although the former mainly projects into the lateral entorhinal cortex (LEC) and the latter mainly projects into the medial entorhinal cortex (MEC) (23). Electrophysiological recordings have found populations of spatially selective "grid cells" in MEC (24), whereas minimal, or only object-related spatial selectivity has been observed in LEC (25–28). This dissociation was recently demonstrated by Hunsaker et al. (29) where lesions of rodent MEC and LEC primarily resulted in selective disruptions in spatial and object discrimination, respectively. It thus appears that the MTL features two largely distinct information streams: an "object" or item stream comprised of PRC and LEC, and a "spatial" or context stream comprised of PHC and MEC. Both streams converge on the DG within the hippocampus, where pattern separation computations are thought to take place. Importantly, strong evidence of domain specificity within the human LEC and MEC has yet to be demonstrated. Full characterization of these "what" and "where" information streams has thus remained elusive in human subjects. Additionally, the respective roles of these information streams in downstream of hippocampal computations are largely unknown.

There is some evidence to suggest that MEC engages in resolution of spatial interference (30), whereas orthogonalization of nonspatial inputs seems to be somewhat dependent on activity in LEC (31). Combined with the largely domain-selective dissociations observed in LEC/MEC lesioned rats in the experiments by Hunsaker et al. (29), these findings suggest that upstream MTL cortices may contribute computational influences that are directly related to pattern separation in the hippocampus in rodent models. However, these contributions have yet to be assessed in humans.

To address this outstanding issue, we used high-resolution functional magnetic resonance imaging (fMRI) (1.5 mm isotropic)

Significance

Episodic memories are complex records of experience, consisting of "what" happened as well as "where" and "when" it happened. Animal studies have demonstrated distinct brain networks supporting memory for information about what experience occurred and information about where the experience occurred. However, such dissociations have been elusive in humans. Using a memory interference task that pits object (i.e., what) vs. spatial (i.e., where) memories against each other and high-resolution fMRI, we report evidence for two parallel but interacting networks in the human hippocampus and its input regions, supporting prior work in animals. We propose a conceptual model of how object and spatial interference are reduced in the regions providing input to the hippocampus, allowing rich, distinct memories to be built.

Author contributions: Z.M.R. and M.A.Y. designed research; Z.M.R. performed research; Z.M.R. analyzed data; and Z.M.R. and M.A.Y. wrote the paper.

The authors declare no conflict of interest.

This article is a PNAS Direct Submission.

[1]To whom correspondence should be addressed. Email: myassa@uci.edu.

This article contains supporting information online at www.pnas.org/lookup/suppl/doi:10.1073/pnas.1411250111/-/DCSupplemental.

to measure activity in hippocampal subfields and surrounding cortices while subjects performed a multidomain mnemonic discrimination task. This task was divided into an encoding phase with an incidental judgment (not overtly mnemonic), and a surprise retrieval phase. In the encoding phase, 18 subjects viewed a series of 260 images of common objects, each appearing in one of 31 possible locations against a 7 × 5 grid (not visible to subjects; *SI Appendix*, Fig. S1*A*), and judged each object as belonging indoors or outdoors and left or right relative to the center of the screen. This spatial grid paradigm has been used by our laboratory to index resolution of spatial interference in young and aged adult humans (32). In the subsequent retrieval phase, subjects were presented with four trial types: repeated images (same object in the same location), object lures (similar object in the original object's location), spatial lures (same object in a different location), and completely novel foil images (Fig. 1*A*). The task included both high- and low-similarity object lures and spatial lures (*SI Appendix*, Fig. S1*B*). Subjects were asked to judge whether each image in this phase featured no change, an object change, a location change, or a novel object, corresponding to each respective trial type. Trials were presented in pseudorandom order, controlling for repetitions of the same trial type and distributed object locations. In this design, we have operationalized mnemonic interference such that a similar lure image is a distortion of the original image. That is, the similar lure image should feature representational overlap with the originally studied image. This overlapping representation should interfere with the original representation in memory, in some cases leading to difficulty in correctly rejecting the lure image. Based on prior work in humans (13–15), it is thought that correct rejection of these similar lures depends at least in part on successful resolution of this interference in the hippocampus.

Because encoding was incidental, our measure of interest was relative engagement of MTL regions as a function of trial type during retrieval. Although there is some evidence to suggest that the nonhuman primate EC receives projections from PRC and PHC in a complex pattern spanning both dorsal/ventral and lateral/medial subdivisions in the EC (22), there is little available data on subdivisions of the human EC. Critically, a recent study by Khan et al. (33) was able to isolate activity in LEC in human subjects and observed age-related aberrations here in concert with findings from rodent and primate models, lending validity to a lateral/medial divide in humans (although this study did not examine task-activated signals). Only one prior study using fMRI in a working memory paradigm found evidence of functional clusters consistent with LEC/MEC distinctions (34). Our approach differs from this study in that our task is designed to tax mnemonic discrimination, thought to rely (at least in part) on hippocampal pattern separation. Given these prior results and the large body of evidence supporting such a division in animals, we focused on distinguishing activity in the lateral and medial portions of the EC as a starting point in delineating the functional division of labor in the EC in humans. We segmented the entorhinal cortex into lateral (LEC) and medial (MEC) portions by using the most inferior white matter at the lateral cortical fold corresponding to the collateral sulcus as a guiding principle for drawing a basic boundary. Please see *Experimental Procedures* and *SI Appendix*, Fig. S8 for a more detailed description of our approach.

Several prior fMRI studies of interference resolution in incidental memory tasks (13, 14) have measured signal adaptation in the DG/CA3 subregion of the hippocampus in response to repeated target items (repetition suppression). In contrast, we designed our task to be explicitly mnemonic during retrieval to examine the dynamics of MTL networks as regions resolved mnemonic interference. As such, correct rejections of lure items in the object and spatial information domains were the trials that were critical to answering our questions. We hypothesized that rejection of object lures would elicit a greater novelty response (resistance to repetition suppression) in PRC and LEC than spatial lures, whereas spatial lures would elicit greater novelty responses in PHC and MEC than object lures. Furthermore, because the DG is thought to undertake pattern separation computations across information domains (2, 35), we hypothesized that correct rejection of either an object or spatial lure would be associated with increased novelty responses in the combined DG/CA3 subregion.

Results

Behavior Is Matched Across Conditions. Lure correct rejection rates did not differ between object and spatial conditions [$F(1,17) = 0.569$, $P = 0.461$] (Fig. 1*B*), and high similarity lures were overall more difficult than low similarity lures [$F(1,17) = 184.61$, $P < 0.001$]. This pattern of results was highly consistent with pilot behavioral data from outside the scanner (*SI Appendix*, Fig. S2). These same basic effects were observed for reaction times (*SI Appendix*, Fig. S3). Critically, these behavioral data demonstrate that difficulty of object and spatial lures were well matched, and that the only factor driving differences in behavior was whether a given lure was of high or low similarity.

Repetition Suppression in DG/CA3. We observed repetition suppression (i.e., adaptation of the BOLD signal with a repeated stimulus) during accurate retrieval of previously studied items

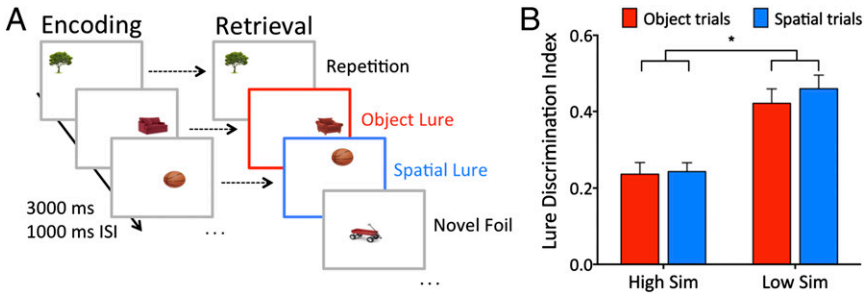

Fig. 1. Object vs. spatial discrimination task and behavioral data. (*A*) Task schematic showing sample displays during the encoding task (concurrent judgment of indoor/outdoor and left/right) and the retrieval task. Object lures vary object identity, whereas spatial lures vary object spatial location. Each item was presented on the screen for 3,000 ms with a 1,000-ms ISI; (*B*) A comparison of performance on high and low similarity object and spatial lure trials. The *y* axis is LDI, which is calculated as p(Object Change|Object Lure) − p(Object Change|Novel Foil) for object lures and p(Spatial Change|Spatial Lure) − p(Spatial Change|Novel Foil). These indices correct for participant response bias. Sample size = 18 subjects. There was a main effect of similarity with high similarity items (both object and spatial) being more difficult to discriminate than low similarity items. There is no main effect of trial type (object vs. spatial) and no interaction between trial type and similarity. Error bars are mean ± SEM. Asterisks indicate significance at $P < 0.05$ corrected.

(i.e., target recognition), which was most pronounced in DG/CA3 (*SI Appendix*, Fig. S4). A one-way ANOVA revealed a significant main effect of region of interest (ROI) in target hits [$F(6,102) = 2.440$, $P = 0.03$]. Consistent with prior findings, DG/CA3 demonstrated greater adaptation than all other ROIs [$F(1,102) = 8.083$, $P < 0.05$ corrected using Scheffé's method].

Correct rejection of novel foils was used as an implicit baseline in our fMRI analyses. As such, deviations from baseline can be generally considered to be memory-related. Functional data from all retrieval trials were subjected to a repeated measures ANOVA with trial type (object lure, spatial lure, or repeat) and ROI (LEC, MEC, PRC, PHC, CA1, Subiculum, and DG/CA3) as fixed factors. These data comprise an abbreviated analysis collapsing across brain hemisphere because no consistent laterality effects were observed, and across lure similarity because activity elicited by high- and low-similarity lures shared highly comparable magnitude and directionality across conditions (for noncollapsed averages, see *SI Appendix*, Fig. S5). The ANOVA revealed a significant main effect of trial type [$F(2,34) = 4.806$, $P = 0.039$ corrected] and a significant main effect of ROI [$F(6,102) = 2.736$, $P = 0.046$ corrected]. We further observed a significant trial type by ROI interaction [$F(12,204) = 6.812$, $P < 0.001$ corrected]. We next performed a series of post hoc contrasts comparing activity within each ROI for each lure domain, using error terms generated by the omnibus F statistic for the aforementioned repeated-measures ANOVA. We corrected for multiple comparisons by using Scheffé's method to adjust our critical F threshold ($F_{\text{Scheffé's}} = 10.799$), and we furthermore corrected for nonsphericity (see *Experimental Procedures* for further details).

LEC Activity Is Selectively Modulated by Object Interference, Whereas MEC Activity Is Modulated by Spatial Interference. LEC was more robustly engaged during object lure discrimination than during spatial lure discrimination [$F(1,102) = 79.539$, $P < 0.05$ corrected] and during target recognition [$F(1,102) = 57.167$, $P < 0.05$ corrected]. Conversely, we found no difference in response magnitude between spatial lures and repeated targets [$F(1,102) = 0.539$, not significant (n.s.)]. These results are shown in Fig. 2*A*. This finding demonstrates that activity the LEC subregion in this study was biased toward mnemonic discrimination based on object identity rather than discrimination based on spatial location or target recognition.

A contrast between object and spatial lure discrimination in MEC did not reach significance under our corrected threshold [$F(1,102) = 7.062$, uncorrected $P = 0.009$]. However, we observed activity in MEC during spatial lure discrimination to be greater than during repetitions [$F(1,102) = 13.896$, $P < 0.05$ corrected], which was not the case for object lures [$F(1,102) = 7.093$, n.s.]. These data are displayed in Fig. 2*D*. We note that this comparison is fairly robust despite our rather conservative correction for multiple comparisons across three trial types and seven ROIs ($F = 7.093$; $F_S = 10.799$). To explore this comparison with a slightly less stringent correction, we ran an additional repeated measures ANOVA with trial type and only MTL cortex ROIs as fixed factors (i.e., excluding the three hippocampal subfields). This analysis yielded a significant main effect of trial type [$F(2,34) = 4.751$, $P = 0.033$ corrected] and a trial type by ROI interaction [$F(6,102) = 8.622$, $P < 0.001$ corrected]. In this case, using Scheffé's method to correct for post hoc comparisons yields a critical $F_S = 6.566$, and our comparison of object lures against spatial lures is significant [$F(1,102) = 8.654$, $P < 0.05$ corrected]. We take these results to suggest that, although less clear than LEC's response profile, MEC is modulated during mnemonic discrimination of spatial information to a greater extent than during discrimination of object information.

To more directly address the central question of opposing domain selectivity in LEC and MEC within our dataset, we performed a condensed repeated measures ANOVA with region (LEC vs. MEC) and domain (object lure vs. spatial lure) as fixed factors. We note that although our LEC and MEC ROIs are

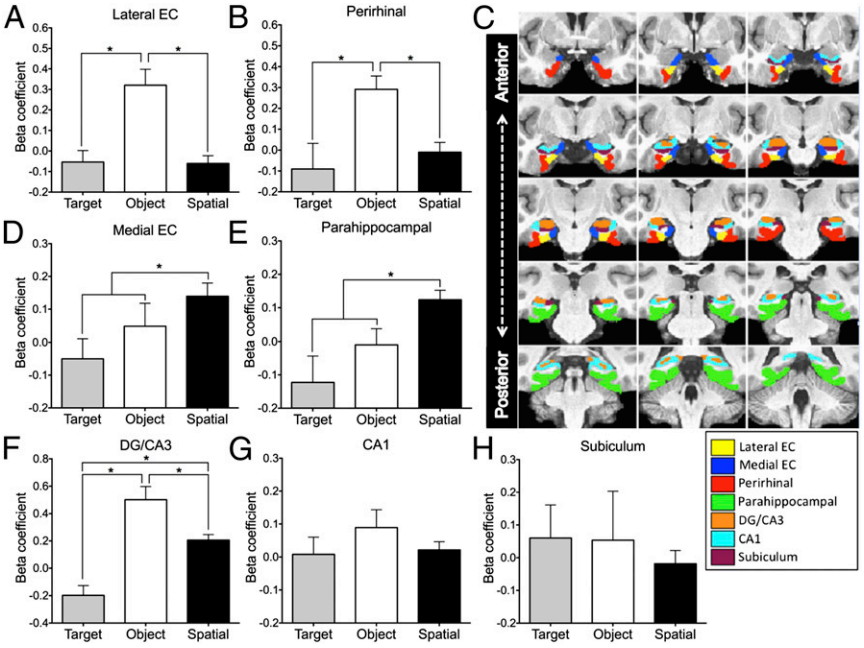

Fig. 2. Region of interest responses during correct rejections of object and spatial lures. (*A* and *B*) Increased activity during object discrimination trials in LEC and PRC. (*C*) ROI segmentation on average group template in the coronal view. Representative slices are arranged from left to right then top to bottom in the anterior-posterior direction, and ROI demarcations are represented in accordance with the color key displayed below. (*D* and *E*) Increased activity during spatial discrimination trials in MEC and PHC. (*F–H*) Increased activity during both object and spatial discrimination trials in DG/CA3 but not in CA1 and subiculum. Baseline (β coefficient = 0) was correct rejection of novel foil images. DG, dentate gyrus; EC, entohrinal cortex. Asterisks indicate significance at $P < 0.05$ corrected.

directly adjacent to one another, different MTL cortices may have different hemodynamic response profiles. Thus, these across-region comparisons must be interpreted with this caveat in mind. This analysis revealed a significant region by domain interaction [$F(1,17) = 20.882$, $P < 0.001$] despite neither a significant effect of region [$F(1,17) = 1.028$, $P = 0.325$] nor domain [$F(1,17) = 3.729$, $P = 0.068$], although we acknowledge that the effect of domain is marginal (*SI Appendix*, Fig. S6*A*). The presence of this interaction in our condensed ANOVA solidifies our aforementioned result of a robust domain-selective dissociation between LEC and MEC in human subjects.

We performed a final analysis over the EC to assess the possibility of an anterior/posterior division of labor rather than lateral vs. medial. Such a division is akin to that performed by Suzuki and Amaral in their investigation of afferent connectivity to the nonhuman primate EC (22). However, with respect to the human EC, there is little anatomical or functional data pertaining to subregional boundaries (also relevant to a potential boundary between the anterior and posterior portions of the region). As such, for our purposes, theirs was done by simply bisecting the extent of the entorhinal portion of the parahippocampal gyrus into anterior and posterior halves. We performed a repeated measures ANOVA over these data with region (anterior vs. posterior EC) and domain (object lure vs. spatial lure) as fixed factors. This analysis did not reveal a significant effect of region [$F(1,17) = 0.553$, $P = 0.467$] or domain [$F(1,17) = 0.018$, $P = 0.896$], and the interaction was not significant [$F(1,17) = 3.306$, $P = 0.1$] (*SI Appendix*, Fig. S6*B*). Thus, a critical domain by region interaction that was significant with a medial/lateral division was not significant when the EC was divided into anterior and posterior portions. A modest, subthreshold interaction was observed, suggesting that there may be some validity to an anterior/posterior specialization within the EC. We note that the data showed considerably less variability within each region and trial type with a lateral/medial segmentation compared with an anterior/posterior segmentation. Together, we take these findings as support for a LEC/MEC division in human subjects, bolstering our aforementioned results.

PRC Activity Is Selectively Modulated by Object Interference, Whereas PHC Activity Is Selectively Modulated by Spatial Interference. Activity in PRC was greater during correct rejection of object lures than spatial lures [$F(1,102) = 63.798$, $P < 0.05$ corrected] and during target recognition [$F(1,102) = 54.866$, $P < 0.05$ corrected]. Furthermore, activity within this region did not differ between rejection of spatial lures and target recognition [$F(1,102) = 4.032$, n.s.]. Like LEC, PRC demonstrates selective engagement during discrimination of object identity (Fig. 2*B*).

We observed the opposite pattern in PHC, which was more active during rejection of spatial lures than object lures [$F(1,102) = 32.246$, $P < 0.05$ corrected] and during target recognition [$F(1,102) = 17.453$, $P < 0.05$ corrected]. Furthermore, activity during rejection of object lures did not differ from repeated targets [$F(1,102) = 6.701$, n.s.]. Thus, PHC shows selective engagement during discrimination of spatial location (Fig. 2*E*).

DG/CA3 Activity Is Modulated by Interference Across Object and Spatial Domains. Consistent with our hypothesis, we found that DG/CA3 was robustly engaged during lure discrimination of both object lures [$F(1,102) = 91.892$, $P < 0.05$ corrected] and spatial lures [$F(1,102) = 67.848$, $P < 0.05$ corrected] relative to recognition of a repeated image. Thus, with novel foils as an implicit baseline, we observed that DG/CA3 was the only region to be significantly more active during correct rejection of both lure modalities than during target recognition, supporting its role in resolution of interfering inputs across domains (Fig. 2*F*). Interestingly, we observed that DG/CA3 was more strongly engaged during rejection of object lures than spatial lures [$F(1,102) = 32.824$, $P < 0.05$ corrected]. Given matched behavioral performance, the reason for this difference is unclear. It bears mentioning that beta coefficients across regions engaged during object lure rejections were generally larger than those observed during spatial lure rejections. This difference may reflect a difference in the nature of mnemonic processing between these two conditions at the neural level that is not apparent in behavioral output. Unlike DG/CA3, we found that activity in CA1 (Fig. 2*G*) and subiculum (Fig. 2*H*) did not differ between any of the respective trial types (all $P > 0.05$). Thus, other hippocampal subfields showed neither domain-specific nor domain-general responsiveness to lure images.

To further explore responses in DG/CA3, we performed across-region comparisons, contrasting DG/CA3 against all other MTL ROIs (LEC, MEC, PRC, PHC, CA1, and subiculum) for both lure domains. As with the interaction analysis between EC subregion and domain as described above, we again note the important caveat that different ROIs likely feature different dynamic ranges of their respective hemodynamic responses. Nonetheless, we found that DG/CA3 was relatively more engaged than other MTL ROIs during correct rejection of object lures [$F(1,102) = 13.935$, $P < 0.05$ corrected] (Fig. 3*A*) and spatial lures [$F(1,102) = 56.702$, $P < 0.05$ corrected] (Fig. 3*B*). Although it is possible that DG/CA3 simply has a larger dynamic range than the other MTL ROIs, we note that beta coefficients in DG/CA3 demonstrated comparable, if not slightly smaller, deviations from baseline during false alarms (*SI Appendix*, Fig. S7). *SI Appendix*, Fig. S6 displays functional activity during false alarms in response to lure images, and although difficult to interpret in itself, can be informative in terms of the overall dynamic range of responses within a region. Thus, this result further suggests a strong role for DG/CA3 in interference resolution across information domains.

We varied lure similarity in this task to assess possible differences in response magnitude at different levels of mnemonic interference. However, in this task, activity in no MTL subregion differed significantly between high- and low-similarity lures. It

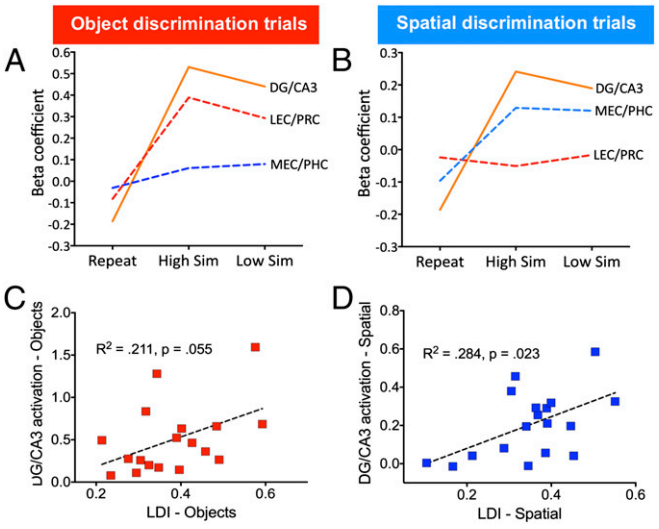

Fig. 3. Activity patterns in DG/CA3 and object vs. spatial input pathways during object and spatial discrimination. (*A*) DG/CA3 shows consistently larger response compared with LEC/PRC and MEC/PHC during object discrimination. LEC/PRC activity was greater than MEC/PHC activity. (*B*) DG/CA3 shows a larger response compared with MEC/PHC and LEC/PRC during spatial lure discrimination. MEC/PHC activity was greater than LEC/PRC activity. (*C*) DG/CA3 activity was marginally predictive of object lure discrimination and was significantly predictive of spatial lure discrimination (*D*). No other MTL subregion showed such a correlation with behavior.

is also worth noting that lure correct rejection signals were generally above baseline (novel foils), suggesting that correctly rejecting similar items produces a larger response in these regions than rejecting completely new items. This issue may be due to an effortful mnemonic process given the explicit nature of the task. Consistent with this account, reaction times on rejection of lure items were significantly longer than rejection of novel foils (*SI Appendix*, Fig. S2).

Activity in DG/CA3 Is Correlated with Lure Discrimination Performance Across Information Domains. Given that the present task assesses mnemonic discrimination across two information domains, we sought to assess the extent to which activity in our ROIs would be behaviorally relevant to either or both judgments. We found DG/CA3 to be the only region with any notable correlations with lure discrimination across subjects. For object discrimination trials, activity in DG/CA3 was marginally (albeit below our significance threshold) correlated with lure discrimination index (LDI) for object lures [$R^2 = 0.211$, $P = 0.055$] (Fig. 3*C*). Additionally, activity DG/CA3 during spatial discrimination was significantly correlated with LDI for spatial lures [$R^2 = 0.284$, $P = 0.023$] (Fig. 3*D*). Thus, despite domain selectivity in LEC and PRC for object information and in MEC and PHC for spatial information, only the DG/CA3 subfield of the hippocampus was significantly correlated with behavior. This result points to a potentially unique role of DG/CA3 in orthogonalizing interfering inputs to influence behavioral output.

Parallel Networks for Object and Spatial Processing. Given the results above, we focused especially on LEC, MEC, PRC, PHC, and DG/CA3 in a series of correlations between ROIs during object or spatial discrimination. These analyses consisted of calculating the extent to which beta coefficients across regions were correlated on a subject-by-subject basis. This set of analyses consisted of 12 comparisons, which were corrected by using Holm's sequentially rejective Bonferroni correction, with an initial critical $P = 0.0042$ and a stepwise decrease in threshold conservatism (36, 37). These analyses are depicted in correlograms in Fig. 4 (for data displaying individual subject scatter plots, see *SI Appendix*, Fig. S8).

During correct rejection of object lures, significant correlations were observed between PRC and LEC [$R^2 = 0.6$, $P = 0.0002$], LEC and DG/CA3 [$R^2 = 0.49$, $P = 0.001$], and PRC and DG/CA3 [$R^2 = 0.47$, $P = 0.0016$], consistent with coupling of the hypothesized object stream. We also observed correlations that were significant between PHC and DG/CA3 [$R^2 = 0.4$, $P = 0.005$] and marginal (via stepwise alpha) between MEC and PHC [$R^2 = 0.32$, $P = 0.014$]. Taken together, these correlations suggest that the spatial network featured relatively less robust functional coupling in these computations than the object network, although MEC and PHC appear to be moderately engaged.

During correct rejection of spatial lures, significant correlations were observed between MEC and PHC [$R^2 = 0.55$, $P = 0.0004$], MEC and DG/CA3 [$R^2 = 0.42$, $P = 0.0036$], and PHC and DG/CA3 [$R^2 = 0.32$, $P = 0.014$], consistent with coupling of the hypothesized spatial stream. No significant correlations were observed between LEC, PRC, and DG/CA3 during correct rejection of spatial lures, suggesting little functional coupling among regions comprising the object network in these computations.

DG/CA3 Shows Differential Responsiveness Along the Hippocampal Longitudinal Axis. We assessed the extent to which the task would drive differences along the hippocampal longitudinal axis with a final analysis to supplement our targeted analyses. Recent work has suggested that the anterior and posterior hippocampus may support dissociable processes (38). We divided the hippocampus into anterior and posterior segments by using the apex of the uncus as a landmark, preserving the segmentation of subregional ROIs (see *SI Appendix*, Fig. S9*A* for a schematic of the

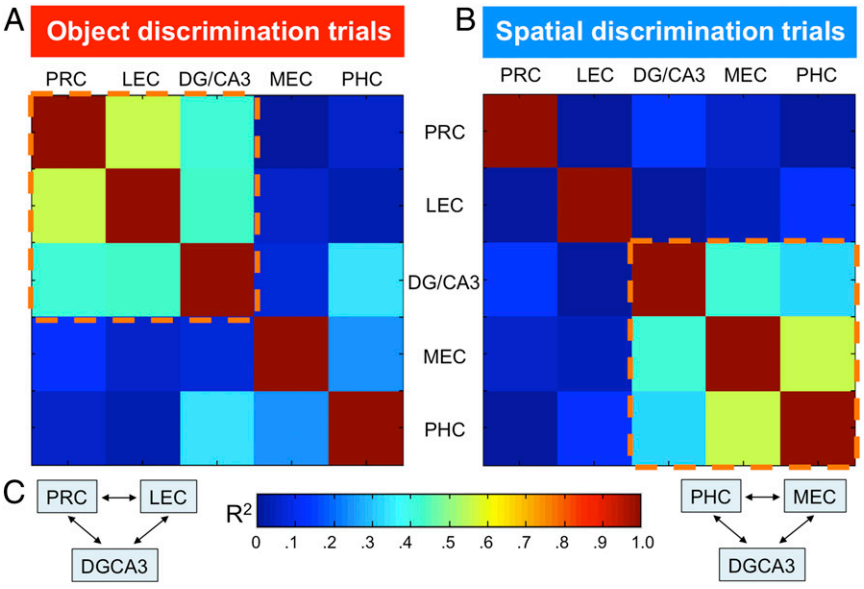

Fig. 4. Regional correlations during object and spatial discrimination trials. (*A*) Pairwise functional correlations between the three regions making up the hypothesized object pathway (LEC, PRC, DG/CA3) during object lure correct rejection trials showing strong coupling among these regions; correlations between the three regions making up the hypothesized spatial pathway (MEC, PHC, DG/CA3) during object lure correct rejection trials showed less correlated activity compared with the object pathway, although perhaps some from functional involvement. (*B*) Pairwise functional correlations between the three regions making up the hypothesized spatial pathway (MEC, PHC, DG/CA3) during spatial lure correct rejection trials showed correlated activity between MEC and PHC and between MEC and DG/CA3; the three regions making up the hypothesized object pathway (LEC, PRC, DG/CA3) during spatial lure correct rejection trials showed virtually no coupling. (*C*) A graphical illustration of the networks that are correlated during object and spatial discrimination trials, which are consistent with our predictions. The series of significance tests over pairwise correlation coefficients were corrected by using Holm's sequentially rejective Bonferroni correction, with an initial critical α of $P < 0.0042$.

delineation point). A repeated measures ANOVA over target hits in hippocampal ROIs (anterior/posterior by region) revealed a significant effect of longitudinal axis [$F(1,17) = 7.718$, $P = 0.013$ corrected] and region [$F(2,17) = 8.964$, $P = 0.001$ corrected], but no interaction [$F(1,17) = 0.612$, $P = 0.548$ corrected]. The effects were driven by greater repetition suppression in anterior DG/CA3, which was significantly larger than in posterior DG/CA3 [$F(1,17) = 20.077$, $P < 0.05$ corrected] (*SI Appendix*, Fig. S9*B*). Thus, the canonical suppression observed in DG/CA3 during the presentation of target images was primarily seen in the anterior portion of DG/CA3 in this experiment.

We next performed the same analyses across ROIs during object and spatial lure correct rejections. For object lures, we only found a significant effect of region [$F(2,17) = 14.283$, $P < 0.001$ corrected], driven by the larger responses in DG/CA3 during object discrimination [$F(1,17) = 24.660$, $P < 0.05$ corrected] (*SI Appendix*, Fig. S9*C*). Thus, DG/CA3 seemed equivalently engaged along the hippocampal longitudinal axis during correct rejection of object lures. For spatial lures, we observed a marginal, nonsignificant effect of longitudinal axis [$F(1,17) = 3.732$, $P = 0.07$ corrected] and an effect of region [$F(1,17) = 7.627$, $P = 0.003$ corrected] (*SI Appendix*, Fig. S9*D*). Although the effect of region is again driven by larger responsiveness in DG/CA3 during spatial lure correct rejections [$F(1,17) = 18.733$, $P < 0.05$ corrected], a direct comparison within DG/CA3 revealed that activity during spatial lures was greater in the posterior portion of the ROI compared with the anterior portion [$F(1,17) = 13.906$, $P < 0.05$ corrected]. This finding lends support to the notion that posterior hippocampal computations may be biased toward spatial/configural processing (39–41) (for a more detailed discussion of such dissociations, see ref. 37).

Discussion

A Hierarchy of Interference Resolution in the Human Medial Temporal Lobe. In line with prior findings across species, our results imply the existence of distinct information streams in the MTL. Like prior human studies, these findings support a functional dissociation between PRC and PHC. However, these results provide previously elusive evidence of such a dissociation between LEC and MEC in human subjects as they resolved object or spatial interference relative to information in memory. Critically, both correlational results and a null interaction in an anterior/posterior division of the EC bolster an LEC/MEC segmentation in human subjects and lend validity to the notion that such a lateral/medial division of the EC exists in the human brain.

Beyond this finding, an important advance made in this study is the ability to examine these distinct networks through their interactions with the hippocampus in the context of one of its core putative computations, pattern separation. These results raise the interesting possibility that interference can be minimized along the hippocampal input pathways as a function of information domain, aiding in powerful orthogonalization that occurs across information domains in DG/CA3. This process is visualized in Fig. 5, which recapitulates our findings and extends our interpretation to this possible network dynamic of incremental reductions in mnemonic interference as information projects to the hippocampus. As is schematized in Fig. 5, extrahippocampal cortices may participate in more basic domain-selective interference resolution, which promote a stronger form of cross-domain resolution to be achieved by the hippocampal DG/CA3 network. As a consequence, perhaps a failure of components of this network to resolve basic interference in a selective domain (e.g., MEC supporting spatial/contextual discriminations) leads to greater difficulty in the hippocampal circuit in performing downstream pattern separation computations. Until recently, it was largely unclear whether upstream computations in MTL cortices are critical for hippocampal orthogonalization, or whether they merely aid in an otherwise efficient process. Given new evidence for a link between LEC and hippocampal pattern separation (31), it seems that MTL cortices play crucial and domain-selective roles in hippocampal computations. Our data are thus consistent with a physiologically plausible mechanism of episodic memory in MTL cortices and hippocampal subfields based on the animal literature, and we extend these ideas to human subjects. Although selective lesions are uncommon and, thus, difficult to study in human subjects, this paradigm can be used to test aged populations in whom the entorhinal cortex (in particular, LEC) is thought to be selectively degraded before the hippocampus itself.

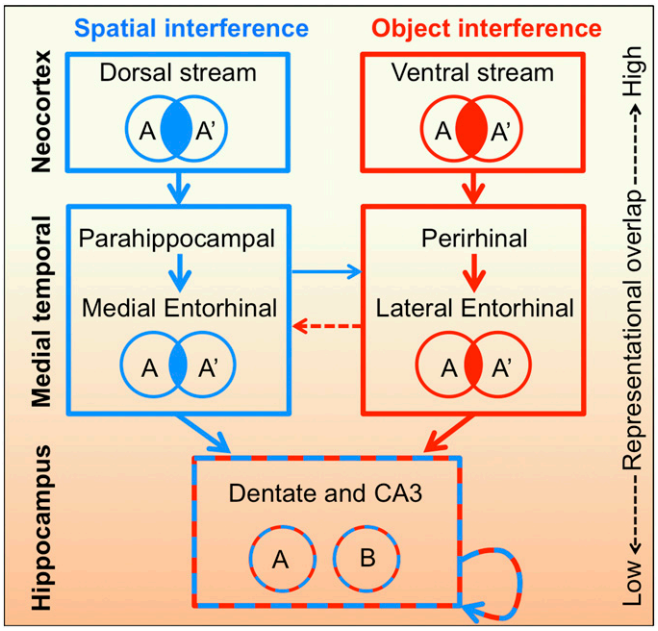

Fig. 5. A hierarchy of mnemonic interference resolution in the medial temporal lobe. The figure illustrates a proposed conceptual model for resolving interference in the medial temporal lobes. The information processing capacities and domain selectivity (object or "nonspatial" processing vs. spatial processing) are based on anatomical connectivity and studies in animals and humans. Given the relative contributions of these regions to the resolution of object and spatial mnemonic interference, we hypothesize that there is an incremental change in domain-selective representational overlap as information proceeds along each pathway to the hippocampal DG/CA3, where representations are multidimensional and maximally separated. The conceptual model amounts to an incremental reduction in mnemonic interference as information projects from domain-selective visual streams into the hippocampus. Critically, there is information exchange at the level of the medial temporal lobe that could potentially integrate information upstream of the hippocampus.

We note that we observed some evidence of regional coupling among regions comprising the spatial network during discrimination of object lures. Many of the changes to object identity in lure items are alterations in shape, size, and/or orientation, which may have engaged the spatial network. We took a narrow definition of spatial discrimination in this study (i.e., metric displacement), and it is certainly possible that spatial processing may pervade neural computations (42). Given the relative magnitude of responses and regional coupling observed in our ROIs, we argue that object discrimination primarily depended on activity in the PRC-LEC network, whereas spatial discrimination primarily depended on activity in the PHC-MEC network in this task. Nonetheless, our data are consistent with anatomical studies suggesting that there is cross-talk and possible cross-modal integration between these functional networks. A related question is whether there are conditions under which these parallel networks operate independently vs. together to influence hippocampal computations. Under normal conditions, the two

networks likely cooperate to confer the correct preliminary signals along both dimensions to the DG/CA3 simultaneously. With the present design, we cannot speak to what happens when information in memory changes along several dimensions at once.

Although we did not observe any condition under which the DG/CA3 was biased toward "completion" rather than "separation," we do not take these data (or other available data) to suggest that pattern separation is the sole modus operandi of the DG/CA3 network. Relative regional activity may be driven by many mnemonic and nonmnemonic processes, and by pattern completion and separation. For example, on a spatial discrimination trial, it is possible that LEC undergoes repetition suppression to the unchanging object features, which creates a contrast with MEC activity (that has not undergone a similar suppression). Thus, the output of this network would be consistent with a spatial pattern separation signal, but may be largely driven by relative completion signals. More generally, in our explicit design, any correct rejection likely involves pattern completion processes, because the original memory must be retrieved to determine whether the current experience differs (i.e., "recall to reject"). Consequently, pattern completion and pattern separation are intertwined and both are probably required for optimal mnemonic processing. It is worth noting, however, that false alarm trials theoretically involve pattern completion computations that are largely absent of pattern separation computations. Thus, if the signal modulations observed during correct rejections were primarily the result of pattern completion, one might expect false alarms to show the same modulations. We actually did not observe this pattern for false alarms (*SI Appendix*, Fig. S6). However, we again note that the explicit memory task used here involves components of both retrieval and mnemonic discrimination, precluding the capture of process-pure computations. Indeed, unlike several prior experiments in this vein (13, 14), activity in DG/CA3 was above baseline during correct rejections, suggesting that lure items were not simply being treated by DG/CA3 as simply "new," as is thought to be the case in incidental tasks.

Although not our aim at the outset of the study, we additionally observed some evidence for a functional dissociation between anterior and posterior hippocampus, specific to the DG/CA3 subfield. A recent review by Poppenk and coworkers (37) extensively discusses the various theories about what may drive such a division. Within our own data, the robust repetition suppression often seen in fMRI studies of the hippocampal DG/CA3 (13, 14) was almost entirely localized to the anterior portion of the subregion. This result may be suggestive of mnemonic functions at the level of basic recognition differing along the hippocampal longitudinal axis, although more targeted experiments will be needed to directly address this possibility. We additionally observed that although object lures equally engaged the anterior and posterior DG/CA3, resolution of spatial interference engaged the posterior portion to a greater extent than the anterior portion. This finding is consistent with the notion that the posterior hippocampus is more biased toward spatial information based on both human fMRI data and electrophysiological recordings in rodents (38–40). However, as previously noted, some of our object lures themselves featured some degree of spatial manipulation. Although the meanings of these anterior/posterior dissociations are beyond the scope of the present study, our data nonetheless suggest that computations related to recognition and mnemonic discrimination may vary as a function of both hippocampal subfield and position along the longitudinal axis of the hippocampus.

Recent human fMRI experiments have found dissociations between PRC and PHC in item and context memory (19, 21, 43–46), although these studies did not manipulate memory interference. Our results are consistent with these data, but extend the findings in two important ways. First, we used a paradigm designed to target pattern separation computations in the hippocampus as a framework for mnemonic processing, allowing us to examine domain-selective regional activity as a function of interference. This approach bridges to studies in rodents where pattern separation has been studied most extensively by using similar paradigms (varying object identity and spatial location). Second, we were able to dissociate domain-selective activity in the human LEC and MEC, the gateway to the hippocampus, and observed that the information content manifesting in PRC and PHC, consistent with anatomical evidence and their purported functional roles. Evidence of a functional division among regions of the human EC and upstream cortical contributions to hippocampal resolution of mnemonic interference resolution critically advances our understanding of basic mnemonic processing in the human MTL.

Experimental Procedures

Participants. Twenty-two right-handed healthy volunteers (13 female; 9 male; mean age of 23.77, SD 1.89) were recruited from the local student community. All participants were screened against major medical or psychiatric morbidities and substance abuse history. Two participants were excluded because of significantly poorer than average performance on the behavioral task. Behavioral performance was subjected to a threshold via d' score (indexing recognition of repeated items; average $d' = 1.42$), which was not allowed to be poorer than the group mean by two SDs. Two additional participants were excluded because of improper functional image alignment (i.e., functional images were acquired with incomplete coverage of the MTL). These exclusions resulted in a final sample of 18 participants (10 female, 8 male; mean age 22.31, SD 1.27). Eighteen participants is a standard sample size for a functional MRI experiment (47), and our analyses were adequately powered to observe the measured effects (observed power > 0.8 for all significant effects, with a two-sided final corrected α of 0.05). Written informed consent was obtained from all participants in accordance with The Johns Hopkins Institutional Review Board, and participants were compensated for their participation.

Study Design. During the encoding phase, object images were presented in one of 31 possible locations on the screen, and subjects were instructed to concurrently judge each object as belonging indoors or outdoors and left or right relative to the center of the screen. During retrieval, subjects were presented with four trial types: repeated images (same object in the same location), object lures (slightly different object in the original object's location), spatial lures (same object in a slightly different location), and novel foil images (Fig. 1*A* and *SI Appendix*, Fig. S1*B*) and were asked to indicate whether the trial showed "No Change," "Object Change," "Location Change," or "New." Each stimulus was presented for 3,000 ms with a 1,000-ms interstimulus interval (ISI).

Stimuli in the behavioral task consisted of 288 pairs of common objects, each pair consisting of two slightly different versions of the same type of object. Object similarity was ranked according to discrimination performance from a large sample of participants ($n > 100$) in a separate study (14). Objects were shown at one of 31 possible locations on a white background, with each location being defined by a space along a 7×5 grid (*SI Appendix*, Fig. S1*A*). These particular dimensions were chosen to accommodate a widescreen resolution while maintaining visibility of the object pictures, because the projector used in the fMRI environment featured a widescreen display.

Objects were randomized across grid positions such that two conditions were satisfied: First, we chose to preclude the occurrence of any object in a corner location, because such trials may have yielded a more salient cue or an anchor during spatial discrimination; second, we ensured that the remaining 31 of 35 grid spaces (corners were avoided because of possible bias as a result of proximity to multiple screen borders) were occupied with roughly equal frequency. Stimuli were displayed via a liquid-crystal display projector reflected in a head-coil mounted mirror. Task presentation and behavioral response collection was conducted within the Psychophysics Toolbox v. 3.0 (48) for MATLAB R2010a (The Mathworks).

In addition to similar object lures, which have been used extensively in our prior investigations of interference resolution in humans (14, 49–51), we designed a set of spatial lures based on varying metric distance (7, 52). We defined a high-similarity lure as an identical object occurring one grid space from its original location, and a low-similarity lure as an identical object occurring two grid spaces from its original location. Performance on these high- and low-similarity spatial lures produced was in the desired accuracy ranges during correct rejections such that high-similarity spatial lures were above chance and were notably more difficult than low-similarity spatial

lures (Fig. 1*B* and *SI Appendix*, Fig. S3). Importantly, the direction of object displacement was counterbalanced when creating the spatial lure stimulus set. For object lures, we sampled stimuli from a preexisting stimulus set with defined mnemonic similarity ratings (14) to create high- and low-similarity identity lures. We compiled a stimulus set in which lure discrimination performance was highly comparable for object and spatial lures, across similarity levels (*SI Appendix*, Fig. S2).

Each of the four trial conditions (Repeat, Object Lure, Spatial Lure, or Foil) featured 72 trials (36 trials of high and low similarity for each lure domain). Images were allocated to a single trial type (i.e., members of each object pair were allocated to a single condition), and assignment of pairs across trial conditions was pseudorandomized across participants. Lure discrimination performance was assessed by using a LDI, which is calculated as p(Object Change|Object Lure) − p(Object Change|Novel Foil) for object lures and p(Spatial Change|Spatial Lure) − p(Spatial Change|Novel Foil). These indices are corrected for response bias. However, this correction necessitates that a different value is subtracted from each respective uncorrected performance value. This procedure may overlook a difference in judgment criterion between object lures and spatial lures that may subtly lead performance levels to differ as a function of trial type. The average p(Object Change|Novel Foil) judgment was 0.105, and the average p(Spatial Change|Novel Foil) judgment was 0.132. Critically, the proportion of such responses did not significantly differ [t (17) = 1.47, $P > 0.05$], suggesting that the decision aspect of subjects' performance was also sufficiently matched. Raw response probabilities are reported in *SI Appendix*, Table S1.

Subjects completed a single scanning session with four functional scans, and a structural magnetization-prepared rapid gradient echo (MP-RAGE) scan. The first two functional scans comprised the encoding phase in which subjects viewed a series of 260 images (130 per run) and were instructed to make an incidental, nonmnemonic judgment about the presented objects. Subjects were tasked with judging each object as belonging indoors or outdoors, and whether each object appeared on the left or the right side of the screen. After the first two scans, the structural scan was acquired (~8 min).

After the structural scan, subjects performed the surprise retrieval phase consisting of 300 images (150 per run) during the final two functional scans. Subjects were instructed to compare each image to those viewed during the encoding phase and were told there would be four types of images presented. The first type was a Repetition, in which subjects saw an identical object to one seen before, and in the same location. The second type was an Object Lure, in which subjects saw a similar, but not identical, object to one seen before, and in the same location as the similar object. The third type was a Spatial Lure, in which subjects saw an identical object to one seen before, but in a similar, not identical location. The final type was a Novel Foil, in which subjects saw a completely new object in a given location on the screen. Subjects were tasked with responding to each respective image as featuring No Change, Object Change, Spatial Change, or New Image via a magnetic resonance-compatible button box.

MRI Data Acquisition. fMRI data were collected by using a 3-Tesla Philips scanner equipped with a SENSE head coil using both higher-order shims and SENSE imaging techniques. Functional images were collected by using a high-speed echo-planar imaging single-shot pulse sequence (1.5 mm isotropic resolution, 19 oblique axial slices parallel to the principal axis of the hippocampus, field of view = 96 × 96 mm, flip angle = 70°, SENSE parallel reduction factor = 2, repetition time (TR)/echo time (TE) = 1500/30 ms, matrix size = 64 × 64).

We additionally collected a novel ultrahigh-resolution structural MPRAGE scan that we developed for accurate delineation of hippocampal subfields and high-resolution diffeomorphic alignment [0.55 mm isotropic resolution; 273 sagittal slices, field of view = 240 × 240 mm, flip angle = 9°, TR/TE = 13/5.9 ms, matrix size = 448 × 448, inversion pulse inversion time (TI) = 1,110 ms]. SENSE parallel imaging was used in two directions (2 × 1.5). The SAR (<10%) and PNS (<75%) were within required limits based on the scanner-calculated values. These scans were also used to create a group template, which was used as the standardized space for alignment of participant data before group analyses.

Image Processing and Analysis. All preprocessing and univariate analyses were conducted by using Analysis of Functional NeuroImages (53). Images were corrected for slice timing and motion, and were detrended across acquisitions by using a first-order (linear) polynomial to further reduce the influence of drift in the scanner signal over time. Time points in which significant motion events occurred (movement exceeded 3° of rotation or 2 mm of translation in any direction relative to prior acquisition ± 1 time point) were censored from analyses. Functional images were coregistered to the structural scans acquired in the same session. Structural scans were aligned to a common template based on the entire sample by using Advanced Normalization Tools (54), which uses Symmetric Normalization to warp individual participants into a common template space. ROIs were drawn manually onto the group template, and each subject's functional data were warped into the common template space for group analysis. This technique has recently been shown to be superior to other traditional nonlinear registration approaches (55). The transformation parameters were then applied to the coplanar functional data, which were then smoothed with a 2.0 mm FWHM Gaussian kernel.

As mentioned in *Results*, our primary measure of interest was correct rejection of object or spatial lures. We chose not to explicitly analyze false alarms, p(No Change|Lure), in this experiment as interpretation of functional signals related to such trials is conceptually challenging. Although it is possible and perhaps even likely that such a judgment is reflective of pattern completion, we cannot confidently conclude that failure to correctly reject a lure reflects this computation, because there are multiple potential sources for this type of error, such as poor attentional allocation during encoding. Behavioral vectors based on trial type (classified according to information domain, similarity, and behavioral decision) were used to model the data by using a deconvolution approach based on multiple linear regression. The resultant fit coefficients (β) estimated activity versus an implicit baseline (correct rejection of novel foils) for a given time point and trial type in a voxel. The sum of the fit coefficients over the expected hemodynamic response (3–12 s after trial onset) was taken as the model's estimate of the response to each trial type (relative to baseline).

Anatomical ROI Segmentations. Hippocampal subfield segmentation was based on our prior work (51, 56), which is defined according to the atlas of Duvernoy (57). The subfields were defined on coronal slices along the anterior–posterior axis of the hippocampus. Representative slices in each hippocampus that best resembled the slices described were chosen and segmented according to the atlas description. The segmentation then proceeded from these slices in both directions slice by slice to ensure a smooth transition across slices. As with prior segmentation protocols, we collapsed activity in the DG and CA3 into a combined DG/CA3 region. Although some recent experiments have reported separate DG and CA3 results, there are several anatomically and functionally informed reasons underlying our decision to avoid this procedure in our own data. First, a fairly sizeable portion of CA3 is in fact encapsulated within DG in the coronal plane, which is extremely difficult (if not altogether impossible) to visually distinguish even with 0.55-mm isotropic structural MRI. Therefore, at 1.5-mm BOLD resolution and given the inherent spatial blur of fMRI data, the validity of separating DG from CA3 signals would be tenuous at best. Second, the anatomy of the two regions is somewhat atypical in that DG granule cells, whereas numerous, fire sparsely, and CA3 pyramidal cells are connected recurrently in a positive feedback network, with both regions under tight inhibitory control (2). Furthermore, from a functional perspective, CA3 activity is likely to conform to separation signals based on input from DG during memory discrimination. These issues are regularly and actively discussed at the Hippocampal Subfield Segmentation Summit meetings (http://hippocampalsubfields.com), an international collaborative effort dedicated to deriving an anatomically validated, unified protocol for hippocampal segmentation on MRI scans.

Segmentations of perirhinal, entorhinal, and parahippocampal cortices proceeded according to the procedures outlined in Insausti et al. (58) and follow our prior work (51, 56). We developed an additional protocol for segmenting the entorhinal cortex into lateral (LEC) and medial (MEC) portions. This procedure was carried out by using the lateral cortical fold forming the apex of the lower bank of the collateral sulcus as a guiding point for bisecting the entorhinal cortex. When performing this segmentation, we attempted to bisect the EC such that the medial and lateral ROIs were designated roughly equal portions of the overall volume of the EC. A divisional boundary was drawn roughly parallel to the apex of the white matter, perpendicular to the medial side of the surface of the EC. As noted in *Results*, this segmentation is a simplification of the anatomical and connective properties of the EC, and little data are available on EC subdivisions in the human. Please see *SI Appendix*, Fig. S10 for a visualization of this particular segmentation. However, given the dissociations observed in the data, we argue that our simplified segmentation is telling of a functional dissociation consistent with animal models. Furthermore, a recent study by Khan et al. (33) isolated aberrant signals in LEC in human subjects in the context of neurocognitive aging, which is highly consistent with selective vulnerability in the analogous EC subregion in rodents. We stress that this delineation explicitly simplifies the anatomy of the EC based on prior work in the primate (22) and, thus, does not fully map onto the many more (as

many as eight) cytoarchitectonic subregions in the human EC (59). There is debate as to whether the human EC features an anterior/posterior split in lieu of or in addition to a medial/lateral division. We performed such an analysis on our data and found that our MEC/LEC division better captured domain-selective variance than an anterior/posterior division (*SI Appendix*, Fig. S9), although a trending interaction is noted. As such, it appears that the human EC may feature a complex hybrid anterolateral/posteromedial division.

Extracting ROI Active Voxels. A functional activity omnibus *F* map (agnostic to condition or trial type) was obtained by setting a voxelwise threshold of $P < 0.2$, and a clusterwise threshold of six voxels. The resulting *F* map was then masked with the structural ROI segmentation map to yield an "active ROI" mask that was then applied to each subject's β-maps to extract condition-specific ROI averages. This procedure essentially yields an anatomical ROI mask that is identical to the full anatomical mask save for a subset of voxels being removed on the basis of liberal functional thresholding. These averages were then subjected to rigorous statistical analyses in the second level, correcting for multiple comparisons and nonsphericity such that the final corrected family-wise α was set at $P < 0.05$. This hybrid structural/functional ROI approach largely, but not wholly, addresses issues with circularity and voxel selection biases (60). That is, this selection procedure is not perfectly orthogonal to subsequent analyses. However, our approach of defining a set of anatomical ROIs a priori greatly reduces statistical biases, and we emphasize that our rather liberal *F*-map threshold retained the vast majority of voxels, and such a procedure is motivated to deselect overly noisy or null voxels to improve power to detect meaningful effects. This strategy is especially pertinent to PRC and EC, which are highly susceptible to noise and signal dropout. Additionally, we emphasize that this approach removes noisy/null voxels across the entire dataset, without respect to whether the significant modulation occurs in response to a particular trial type. Critically, we are nevertheless blinded as to whether a given voxel is selectively responsive to a target, an object lure, or a spatial lure. Voxel betas from the resulting hybrid functional/structural ROIs were averaged, and all subsequent statistical analyses were conducted on these averages.

Statistical Analyses. All statistical analyses of behavioral variables and ROI activation means were conducted in SPSS v. 20.0 (IBM, released 2011). Statistical tests were corrected for multiple comparisons by using Scheffé's correction where appropriate. All tests used the General Linear Model (ANOVA and correlations). Statistical values were considered significant at an α level of 0.05 and were corrected when appropriate to control for type I error.

Statistical testing of fMRI data were first performed by using a two-way repeated measures ANOVA (trial type × ROI) to assess significant main effects and interaction across the dataset. Post hoc comparisons among trial conditions or region following a significant ANOVA were conducted by using contrasts. Contrasts weigh the means of respective conditions to generate a sum of squares for each comparison, which is divided by the appropriate error term (i.e., the term for the interaction or a particular main effect, depending on the comparison being run) from the omnibus ANOVA to generate an *F* statistic. These analyses are more appropriate than post hoc *t* tests following an ANOVA, because contrasts operate over the same variance space as the observed *F* statistic. This approach eliminates experimenter bias in such analyses because the variance space of the comparison at hand is not selectively limited. Contrasts furthermore allow for correction of nonsphericity in post hoc comparisons. The omnibus ANOVA and post hoc contrasts were Greenhouse–Geisser corrected for nonsphericity. This correction is important, because analyses over a general linear model assume independent and identically distributed error (i.e., sphericity). This assumption of sphericity is in fact often violated, and in such cases correction is appropriate. All post hoc comparisons were corrected for α inflation by using Scheffé's method, which adjusts the critical *F* statistic for contrasts on the basis of the number of conditions modeled in a given ANOVA (i.e., $F_{\text{Scheffé's}} = F_{\text{initial}} \times N_{\text{conditions}} - 1$). All correlational analyses were corrected for a given family of data by using Holm's sequentially rejective Bonferroni correction, which has an initial critical *P* value equal to a Bonferroni correction and becomes less conservative in a stepwise fashion. Tests reported as being significant surpassed the adjusted threshold.

ACKNOWLEDGMENTS. We thank Raymond Kesner, Jim Knierim, Michela Gallagher, Craig Stark, and Sarah Morse for helpful discussions and comments on earlier versions of this manuscript and Liz Murray and Kristen Thompson for help with participant recruitment and testing. This study was supported by National Institute on Aging Grants P50 AG05146 and R01 AG034613 and National Science Foundation Graduate Research Fellowship DGE1232825.

1. Milner B, Squire LR, Kandel ER (1998) Cognitive neuroscience and the study of memory. *Neuron* 20(3):445–468.
2. Yassa MA, Stark CEL (2011) Pattern separation in the hippocampus. *Trends Neurosci* 34(10):515–525.
3. Marr D (1971) Simple memory: A theory for archicortex. *Philos Trans R Soc Lond B Biol Sci* 262(841):23–81.
4. McClelland JL, McNaughton BL, O'Reilly RC (1995) Why there are complementary learning systems in the hippocampus and neocortex: Insights from the successes and failures of connectionist models of learning and memory. *Psychol Rev* 102(3): 419–457.
5. Treves A, Rolls ET (1994) Computational analysis of the role of the hippocampus in memory. *Hippocampus* 4(3):374–391.
6. O'Reilly RC, Norman KA (2002) Hippocampal and neocortical contributions to memory: Advances in the complementary learning systems framework. *Trends Cogn Sci* 6(12):505–510.
7. Hunsaker MR, Rosenberg JS, Kesner RP (2008) The role of the dentate gyrus, CA3a,b, and CA3c for detecting spatial and environmental novelty. *Hippocampus* 18(10): 1064–1073.
8. Kesner RP, Lee I, Gilbert P (2004) A behavioral assessment of hippocampal function based on a subregional analysis. *Rev Neurosci* 15(5):333–351.
9. Gilbert PE, Kesner RP, Lee I (2001) Dissociating hippocampal subregions: Double dissociation between dentate gyrus and CA1. *Hippocampus* 11(6):626–636.
10. McHugh TJ, et al. (2007) Dentate gyrus NMDA receptors mediate rapid pattern separation in the hippocampal network. *Science* 317(5834):94–99.
11. Leutgeb JK, Leutgeb S, Moser M-B, Moser EI (2007) Pattern separation in the dentate gyrus and CA3 of the hippocampus. *Science* 315(5814):961–966.
12. Neunuebel JP, Knierim JJ (2014) CA3 retrieves coherent representations from degraded input: Direct evidence for CA3 pattern completion and dentate gyrus pattern separation. *Neuron* 81(2):416–427.
13. Bakker A, Kirwan CB, Miller M, Stark CEL (2008) Pattern separation in the human hippocampal CA3 and dentate gyrus. *Science* 319(5870):1640–1642.
14. Lacy JW, Yassa MA, Stark SM, Muftuler LT, Stark CEL (2011) Distinct pattern separation related transfer functions in human CA3/dentate and CA1 revealed using high-resolution fMRI and variable mnemonic similarity. *Learn Mem* 18(1):15–18.
15. LaRocque KF, Smith ME, Carr VA, Witthoft N, Gill-Spector K, Wagner AD (2013) Global similarity and pattern separation in the human medial temporal lobe predict subsequent memory. *J Neurosci* 33(13):5466–5474.
16. Norman G, Eacott MJ (2005) Dissociable effects of lesions to the perirhinal cortex and the postrhinal cortex on memory for context and objects in rats. *Behav Neurosci* 119(2):557–566.
17. Eacott MJ, Gaffan EA (2005) The roles of perirhinal cortex, postrhinal cortex, and the fornix in memory for objects, contexts, and events in the rat. *Q J Exp Psychol B* 58(3-4): 202–217.
18. Gaffan EA, Healey AN, Eacott MJ (2004) Objects and positions in visual scenes: Effects of perirhinal and postrhinal cortex lesions in the rat. *Behav Neurosci* 118(5):992–1010.
19. Diana RA, Yonelinas AP, Ranganath C (2012) Adaptation to cognitive context and item information in the medial temporal lobes. *Neuropsychologia* 50(13): 3062–3069.
20. Diana RA, Yonelinas AP, Ranganath C (2007) Imaging recollection and familiarity in the medial temporal lobe: A three-component model. *Trends Cogn Sci* 11(9):379–386.
21. Staresina BP, Duncan KD, Davachi L (2011) Perirhinal and parahippocampal cortices differentially contribute to later recollection of object- and scene-related event details. *J Neurosci* 31(24):8739–8747.
22. Suzuki WA, Amaral DG (1994) Perirhinal and parahippocampal cortices of the macaque monkey: Cortical afferents. *J Comp Neurol* 350(4):497–533.
23. Witter MP, Wouterlood FG, Naber PA, Van Haeften T (2000) Anatomical organization of the parahippocampal-hippocampal network. *Ann N Y Acad Sci* 911:1–24.
24. Hafting T, Fyhn M, Molden S, Moser M-B, Moser EI (2005) Microstructure of a spatial map in the entorhinal cortex. *Nature* 436(7052):801–806.
25. Deshmukh SS, Knierim JJ (2011) Representation of non-spatial and spatial information in the lateral entorhinal cortex. *Front Behav Neurosci* 5:69.
26. Yoganarasimha D, Rao G, Knierim JJ (2011) Lateral entorhinal neurons are not spatially selective in cue-rich environments. *Hippocampus* 21(12):1363–1374.
27. Tsao A, Moser M-B, Moser EI (2013) Traces of experience in the lateral entorhinal cortex. *Curr Biol* 23(5):399–405.
28. Hargreaves EL, Rao G, Lee I, Knierim JJ (2005) Major dissociation between medial and lateral entorhinal input to dorsal hippocampus. *Science* 308(5729):1792–1794.
29. Hunsaker MR, Chen V, Tran GT, Kesner RP (2013) The medial and lateral entorhinal cortex both contribute to contextual and item recognition memory: A test of the binding of items and context model. *Hippocampus* 23(5):380–391.
30. Fyhn M, Hafting T, Treves A, Moser M-B, Moser EI (2007) Hippocampal remapping and grid realignment in entorhinal cortex. *Nature* 446(7132):190–194.
31. Lu L, et al. (2013) Impaired hippocampal rate coding after lesions of the lateral entorhinal cortex. *Nat Neurosci* 16(8):1085–1093.

32. Reagh ZM, et al. (2014) Spatial discrimination deficits as a function of mnemonic interference in aged adults with and without memory impairment. *Hippocampus* 24(3):303–314.
33. Khan UA, et al. (2014) Molecular drivers and cortical spread of lateral entorhinal cortex dysfunction in preclinical Alzheimer's disease. *Nat Neurosci* 17(2):304–311.
34. Schultz H, Sommer T, Peters J (2012) Direct evidence for domain-sensitive functional subregions in human entorhinal cortex. *J Neurosci* 32(14):4716–4723.
35. Azab M, Stark SM, Stark CEL (2013) Contributions of human hippocampal subfields to spatial and temporal pattern separation. *Hippocampus* 24(3):293–302.
36. Holm S (1979) A simple sequentially rejective multiple test procedure. *Scand J Stat* 6:65–70.
37. Holland BS, Copenhaver MD (1987) An improved sequentially rejective Bonferroni test procedure. *Biometrics* 43:417–423.
38. Poppenk J, Evensmoen HR, Moscovitch M, Nadel L (2013) Long-axis specialization of the human hippocampus. *Trends Cogn Sci* 17(5):230–240.
39. Jung MW, Wiener SI, McNaughton BL (1994) Comparison of spatial firing characteristics of units in dorsal and ventral hippocampus of the rat. *J Neurosci* 14(12): 7347–7356.
40. Hirshhorn M, Grady C, Rosenbaum RS, Winocur G, Moscovitch M (2012) Brain regions involved in the retrieval of spatial and episodic details associated with a familiar environment: An fMRI study. *Neuropsychologia* 50(13):3094–3106.
41. Ryan L, Lin CY, Ketcham K, Nadel L (2010) The role of medial temporal lobe in retrieving spatial and nonspatial relations from episodic and semantic memory. *Hippocampus* 20(1):11–18.
42. O'Keefe J, Nadel L (1978) *The Hippocampus as a Cognitive Map* (Oxford Univ Press, Oxford).
43. Watson HC, Lee ACH (2013) The perirhinal cortex and recognition memory interference. *J Neurosci* 33(9):4192–4200.
44. Diana RA, Yonelinas AP, Ranganath C (2010) Medial temporal lobe activity during source retrieval reflects information type, not memory strength. *J Cogn Neurosci* 22(8):1808–1818.
45. Hannula DE, Libby LA, Yonelinas AP, Ranganath C (2013) Medial temporal lobe contributions to cued retrieval of items and contexts. *Neuropsychologia* 51(12):2322–2332.
46. Sadeh T, Maril A, Bitan T, Goshen-Gottstein Y (2012) Putting Humpty together and pulling him apart: Accessing and unbinding the hippocampal item-context engram. *Neuroimage* 60(1):808–817.
47. Murphy K, Garavan H (2004) An empirical investigation into the number of subjects required for an event-related fMRI study. *Neuroimage* 22(2):879–885.
48. Brainard DH (1997) The psychophysics toolbox. *Spat Vis* 10(4):433–436.
49. Yassa MA, et al. (2011) Pattern separation deficits associated with increased hippocampal CA3 and dentate gyrus activity in nondemented older adults. *Hippocampus* 21(9):968–979.
50. Yassa MA, et al. (2010) High-resolution structural and functional MRI of hippocampal CA3 and dentate gyrus in patients with amnestic mild cognitive impairment. *Neuroimage* 51(3):1242–1252.
51. Yassa MA, Mattfeld AT, Stark SM, Stark CEL (2011) Age-related memory deficits linked to circuit-specific disruptions in the hippocampus. *Proc Natl Acad Sci USA* 108(21):8873–8878.
52. Stark SM, Yassa MA, Stark CEL (2010) Individual differences in spatial pattern separation performance associated with healthy aging in humans. *Learn Mem* 17(6): 284–288.
53. Cox RW (1996) AFNI: Software for analysis and visualization of functional magnetic resonance neuroimages. *Comput Biomed Res* 29(3):162–173.
54. Avants BB, et al. (2011) A reproducible evaluation of ANTs similarity metric performance in brain image registration. *Neuroimage* 54(3):2033–2044.
55. Klein A, et al. (2009) Evaluation of 14 nonlinear deformation algorithms applied to human brain MRI registration. *Neuroimage* 46(3):786–802.
56. Yassa MA, Stark CEL (2009) A quantitative evaluation of cross-participant registration techniques for MRI studies of the medial temporal lobe. *Neuroimage* 44(2):319–327.
57. Duvernoy H (1998) *The Human Hippocampus: Functional Anatomy, Vascularization, and Serial Sections with MRI* (Springer, Berlin).
58. Insausti R, et al. (1998) MR volumetric analysis of the human entorhinal, perirhinal, and temporopolar cortices. *AJNR Am J Neuroradiol* 19(4):659–671.
59. Insausti R, Tuñón T, Sobreviela T, Insausti AM, Gonzalo LM (1995) The human entorhinal cortex: A cytoarchitectonic analysis. *J Comp Neurol* 355(2):171–198.
60. Kriegeskorte N, Simmons WK, Bellgowan PSF, Baker CI (2009) Circular analysis in systems neuroscience: The dangers of double dipping. *Nat Neurosci* 12(5):535–540.